

# Bread dough rheology in biaxial and step-shear deformations

Roger I. Tanner · Shao-Cong Dai · Fuzhong Qi

Received: 20 August 2007 / Accepted: 11 December 2007 / Published online: 29 January 2008  
© Springer-Verlag 2007

**Abstract** We consider the use of a Lodge-type model with a damage function for the description of some bread dough rheology. The model has been reasonably successful in uniaxial elongation and shearing, and here, we investigate biaxial stretching, using a bubble method, and some step strain shear motions. The damage function, previously regarded as a function of the largest Hencky strain, is shown to be inadequate to describe biaxial stretching, and a modification is proposed. The sequence of step strains, with both reversing and steadily increasing steps, is reasonably well described by the model. The revised model can therefore describe small-strain motions, steady shearing, steady uniaxial and biaxial elongations, recoil, stress relaxation and step strain motions.

**Keywords** Dough rheology · Uniaxial elongation · Biaxial extension · Bubble technique · Step shear · Damage function · Lodge’s model · Maxwell model

## Introduction—the damage function concept

Dough rheology plays an important role in determining the processing behaviour and final quality of baked products (Bloksma 1990), and the search for a relatively simple rheological model of bread dough continues. Dough is not a simple material; it is a polymeric network with about 60% by volume of starch filler particles, and constitutive models for such materials are still being sought.

It has been suggested (Tanner et al. 2007, 2008; Qi et al. 2008) that some varieties of bread dough exhibit rheology that can be described using a modified Lodge-type (Lodge 1964) model incorporating a “damage” function, which accounts for the observed reduction in stresses below those computed using the original Lodge model. For the Australian hard wheat JANZ variety (Qi et al. 2008; Tanner et al. 2008) it was suggested that the following model was useful.

$$\boldsymbol{\sigma} = -p\mathbf{I} + f \int_{-\infty}^t m(t-t')\mathbf{C}^{-1}(t')dt' \quad (1)$$

In this equation,  $\boldsymbol{\sigma}$  is the total stress tensor,  $m$  is a memory function and  $\mathbf{C}^{-1}(t')$  is the Finger strain tensor at time  $t'$ , computed relative to the configuration at time  $t$ . The material is assumed to be incompressible, so the pressure term— $p\mathbf{I}$ —has to be found from the balance of momentum. If  $f=1$ , then Eq. 1 is Lodge’s rubber-like liquid model (Lodge 1964); we have suggested that the damage function  $f$  is only a function of the largest Hencky strain, where the Hencky strain  $\varepsilon_H$  is assumed to be measured from some initial configuration before deformation begins. For the JANZ wheat varieties considered here, the small-strain oscillation behaviour suggests a simple power-law form for  $m$ :

$$m(t) = pG(1)t^{-(1+p)} \quad (2)$$

where  $p$  is in the range 0.2–0.3 and  $G(1)$  is a constant.

The damage function  $f$  in Eq. 1 has to be found from experiments; it was found (Tanner et al. 2007, 2008) that it could be represented for a certain dough as a function only of the Hencky strain measured from the initial rest state; the larger the strain, the smaller is  $f$ . The damage function model thus shows reduced stresses compared to the Lodge

R. I. Tanner (✉) · S.-C. Dai · F. Qi  
School of Aerospace, Mechanical and Mechatronic Engineering,  
University of Sydney,  
Sydney, NSW 2006, Australia  
e-mail: rit@aeromech.usyd.edu.au

model, where  $f=1$ . It was found, in our previous work, for the JANZ wheat used there that using Eqs. 1 and 2 with a damage function  $f$  of the form (for  $\varepsilon_H \lesssim 3$ )

$$f = \left\{ \frac{1}{1.0953 + (111.74\varepsilon_H)^{1.1026}} - 0.0225\varepsilon_H + 0.087 \right\} e^{-(0.32\varepsilon_H)^{30}} \quad (3)$$

was useful (Tanner et al. 2008). Note that linear viscoelastic behaviour in bread dough occurs only for small strains of order  $10^{-3}$  as is well-known (for example, see Hibberd and Wallace 1966; Tanner et al. 2008). Equation 3 was designed to describe the type of behaviour seen in Fig. 1.

For  $\varepsilon_H \gtrsim 3$ , fracture occurs, and  $f$  rapidly approaches zero; this is the reason for the last term on the right hand side of Eq. 3. In Eq. 3, when  $\varepsilon_H=0$ ,  $f=1.0$ , as expected, and a very rapid reduction in stress occurs as  $\varepsilon_H$  increases: for

example when  $\varepsilon_H=0.1$ ,  $f \approx 0.15$ . For larger  $\varepsilon_H$  values,  $f$  is nearly linear in  $\varepsilon_H$ . For example, at  $\varepsilon_H=1$ ,  $f=0.07$ .

Using the above set of relations, we found (Tanner et al. 2007, 2008) that shear and elongation beginning from rest could be adequately described. The small-strain behaviour was built-in to the model (Eq. 2), so that was also well described.

In addition, relaxation after a sudden step of shear and recoil after elongation were well described; the behaviour in medium-sized oscillatory flows ( $\sim 10\%$  strain) was fairly well described, and an application to sheeting problems was also successful (Qi et al. 2008). However, the model obviously needs more extensive testing in different deformation patterns, and the present paper reports some biaxial test results and also step strain results. We note that uniaxial and biaxial stretching are extremes in the deformation patterns, as discussed by Bird et al. (1987). The object of the biaxial tests is to see if these can be described using the simple  $f(\varepsilon_H)$  damage function devised for tests in shear and uniaxial elongation. The point of the step shear strain sequence tests is to check whether “healing” of the damaged specimen occurs during a rest between step strains. Hibberd and Wallace (1966) used sinusoidal strains of varying amplitude and noted rapid strain softening upon initial straining and a very slow and incomplete recovery after suddenly changing strain amplitudes from  $O(10^{-3})$  to  $O(10^{-2})$  and back again; times of testing and (partial) recovery extended to 4 h. The present work uses larger ( $O(10^{-1})$ ) shear strains and shorter intervals up to 1 h.

The dough used here was a similar wheat breed to the JANZ material used formerly, but it was from a different batch of flour; mixing procedures followed the pattern described previously (Tanner et al. 2008).

We found, from relaxation tests after a step of shear strain of 0.1% magnitude,  $p=0.22$  and  $G(1) \sim 14.2$  kPa  $s^p$  for the new batch of flour, and the  $f$  function was found from relaxation measurements at larger strain steps and steady shearing to be well fitted by (Fig. 1a,b)

$$\begin{aligned} f &= -0.227 \log \varepsilon_H + 0.092 & (\varepsilon_H \leq 1.0) \\ f &= -0.1542 \log \varepsilon_H + 0.092 & (\varepsilon_H > 1.0) \end{aligned} \quad (4)$$

Equation 4 is a more convenient form than Eq. 3; they are in any case for different batches of dough, and both model the drastic reduction in  $f$  for small strains. These values were used in the following computations; see also Tanner et al. (2007) for details of the single-step relaxation tests.

Ng et al. (2006) have also used a Lodge model with a memory function of form (2). They speak of a “damping function” obtained in shear, which seems to imply the use of a Wagner model (Tanner 2000). However, their analysis

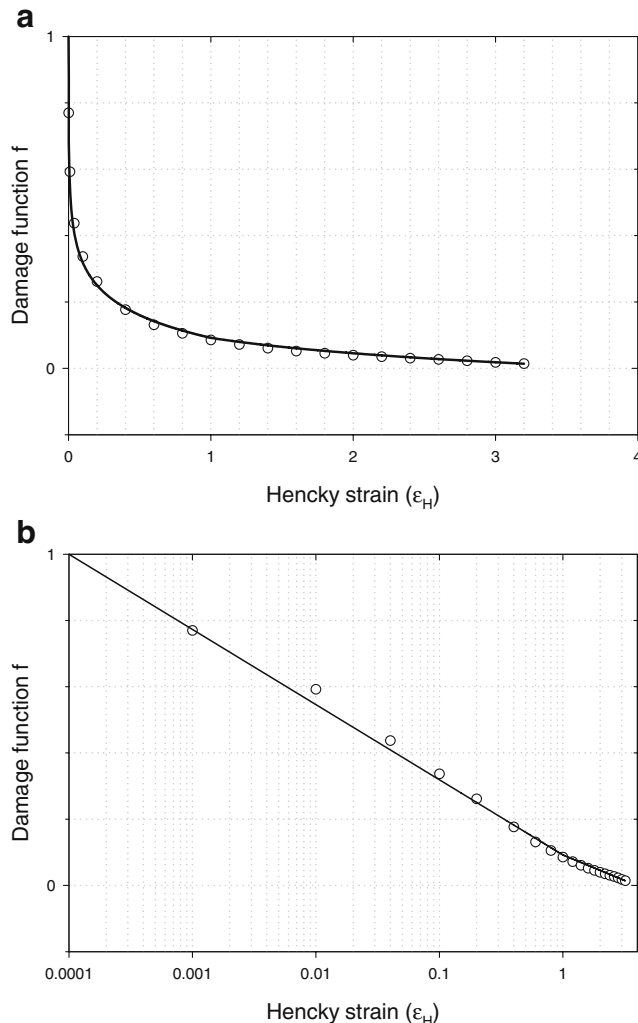


**Fig. 1** **a** Damage function  $f$  for JANZ dough as a function of Hencky strain  $\varepsilon_H$  deduced from steady shearing. For  $\varepsilon_H > 3$ ,  $f$  rapidly reduces to zero. **b** Damage function on an expanded scale at lower strains. Results were deduced from stress relaxation in shear. The curves were fitted by Eq. 4

is incomplete and does not, we believe, imply the use of a damage function in our sense.

## Preparations and experimental measurements

### Dough preparation

The material used for this study was Bake Extra Flour<sup>®</sup>, a commercial Australian flour (Table 1). The dough was produced in a 10-g mixograph by mixing 200 mg of salt, 6.0 g of distilled water and 9.5 g of flour, as determined by using a Sartorius<sup>®</sup> digital high-precision scale. The sample was mixed by four planetary pins on the head revolving around three stationary pins on the bottom of the mixing bowl at a speed of 71 rpm. The mixing operation was conducted at a temperature of 24 °C and under ambient humidity in an air-conditioned laboratory. The mixing time was about 3 min at which the mixing curves peaked and the dough was developed. The mixed dough was stored in a sealed bag to relax for 45 min before testing.

### Dough-inflating (bubble) measurements

For the dough-inflating (biaxial strain) measurements, the mixed dough was made into a 1.8-mm-thick sheet using a compression mould. Before compressing, the mixed dough was sandwiched between two sheets of transparency film with a thin coating of 100 cSt silicone oil. With a film sheet on the top and bottom, the dough was rolled to approximately 5 mm thickness in such a way that the silicone oil was evenly coated on both sides of the dough sheet to prevent the sample from drying. Together with the two sheets of film, the dough was moved into the compression mould, and the mould was calibrated so that the dough would be compressed to a thickness of approximately 1.8 mm. The dough was kept in the compression mould for 45 min.

For this study, the large deformation of spherical and “rectangular” dough bubbles was measured. The bubble inflation device was designed and built, following Charalambides et al. (2002a) as showed in Fig. 2. The chamber was made using an aluminum tube with a 25×25×1.5 mm thick square hollow section. A steel bottom plate

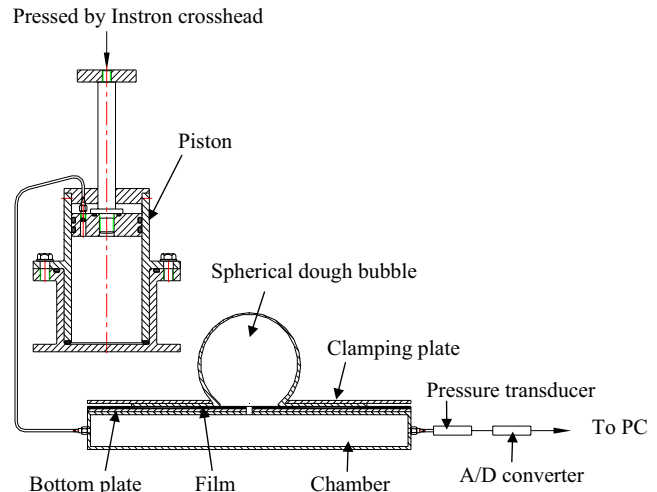


**Fig. 2** The bubble inflation system. The initial radius of the sheet for spherical bubble was 25 mm. For the rectangle (“sausage”) bubble, the initial sheet area was 120×30 mm

was fixed on the chamber, and a sheet of transparency film was stuck to the bottom plate to ensure that the contact surface between the dough and the bottom plate was smooth. The size of the air hole that was on the top of the chamber had a 4-mm diameter for the spherical bubble and dimensions of 80×2 mm for the rectangular bubble. The purpose of the air hole is to allow the compressed air generated by the Instron crosshead pressing the piston to inflate the dough sample. The size of the bubble-based hole in the clamping plate was 50 mm diameter for the spherical bubble and dimensions of 120×30 mm for the rectangular bubble. Before inserting the dough sheet, a thin coating of paraffin oil was applied as a lubricant on the bottom plate film surface, and the dough sheet was carefully moved on to it. Then, a net was placed on the dough sheet. Paint was air brushed through the net onto the top surface of the dough sheet yielding grids with dimensions of 1.45×1.0 mm, and the gridlines were 0.2 mm in width. Therefore, the centre distances are 1.65 mm lengthwise and 1.2 mm widthwise between two consecutive painted grid lines. In testing, the piston was mounted on the Instron 4302 testing machine. The Instron crosshead pressed the piston to generate compressed air at the speed of 50 mm/min, thus inflating the dough sample. The pressure inside the bubble was detected by a 50-mbar pressure transducer (HCXM050D6V Farnell). The calibration of the pressure transducer was carried out using a U-tube manometer, and the input signals were calibrated before testing. The measured signals were transferred to PC by an A/D converter (Dataq DI 194 RS). The deformation of the expanding dough bubble was recorded by two digital cameras from the top and horizontal views, respectively. Calibration curves for correcting the geometrical measurements because of variations in distance from the lenses were obtained by measuring a fixed

**Table 1** Physiochemical properties of <sup>®</sup>Bake Extra Flour

Property	Amount
Protein	12.9%
Unextractable polymeric protein	41.89%
Optimal water addition	63.16%
Optimal mixing time	3.00 min

length on the scales that were laid at different distances from the camera lenses. The displacement of piston vs time was directly recorded by the Instron 4302. For the thickness measurements, the true initial thickness of the dough sheet was calculated by the measured density and the weight of the circular disks that were cut using a 10.4-mm diameter cutter before inflating. The top thicknesses of the bubbles were calculated by assuming the dough is incompressible and by dividing the initial volume of the dough sheet with a cross-section of  $1.65 \times 1.2$  mm by the product of the measured stretched distances of the expanding bubble in length and in width. Then the stresses on the top of the bubble could be calculated, as described in “Biaxial testing” below.

### Relaxation measurements

The relaxation measurements were conducted on a Paar Physica MCR 301 controlled stress rheometer. Parallel plates with a diameter of 25 mm were used, and the gap was set to 2 mm for the measurements. Sandpaper was glued to the parallel plates to prevent the dough from slipping, and the calibration for the rheometer was performed before testing. Then, the sample was mounted on the lower plate and compressed between the plates by moving down the upper plate to a set gap. Excess dough was trimmed, and the edge of the sample was coated with Shell® petroleum jelly to prevent moisture loss. After that, the sample was allowed to relax for a further period of 45 min. Two measuring profiles were set: One is that during continuous testing, a step strain of 10% was applied on the sample, and the relaxation time was 100 s, then, a reverse step was applied so the total strain was zero, with a relaxation time of 100 s, as shown in Fig. 11. The other profile used applied a series of 10% strain steps. The sample was deformed by a step strain of 10%, and then, a relaxation time of 1,000 s occurred, then the test was continued with a 10% strain increase, i.e. 20% strain, and a relaxation time of 1,000 s, as shown in Fig. 15.

### Biaxial testing

To produce a biaxial strain field, we used ‘bubble’ techniques, similar to those reported by Charalambides et al. (2002a, b, 2006) and others (Dobraszczyk and Morgenstern 2003). For a thin shell of dough, subjected to an internal pressure  $\Delta p$ , then at a given location, if the local thickness is  $\delta$ , and the two radii of curvature are  $\rho_1$  and  $\rho_2$ , respectively, with corresponding stresses  $\sigma_1$  and  $\sigma_2$ , then one has (Tanner 2000; see Fig. 3)

$$\frac{\Delta p}{\delta} = \frac{\sigma_1}{\rho_1} + \frac{\sigma_2}{\rho_2} \quad (5)$$

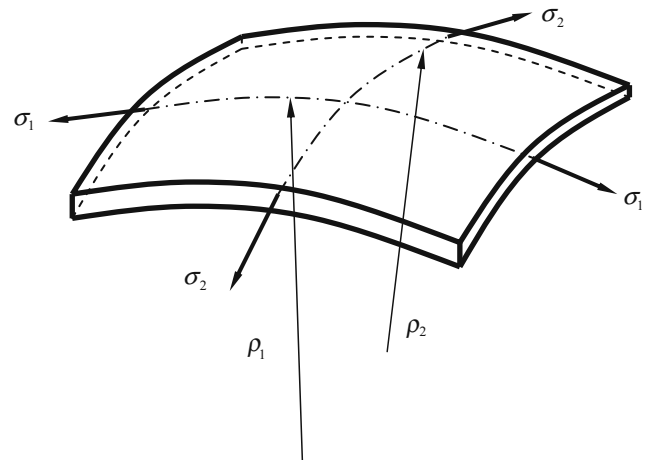


**Fig. 3** Thin shell principal curvatures ( $\rho_1, \rho_2$ ) and stresses ( $\sigma_1, \sigma_2$ ) in a small element. The pressure acts on the lower side and the local thickness is  $\delta$

For a near-spherical bubble (Fig. 4), we have the conditions:  $\sigma_1 = \sigma_2 = \sigma$  and  $\rho_1 = \rho_2 = R$ , where  $R$  is the radius of the curvature at the pole or top of the bubble. The stress is therefore obtained by

$$\sigma = \frac{(\Delta p)R}{2\delta} \quad (6)$$

The deformation at the pole is purely biaxial in this case. We also have used a rectangular or “Sausage” bubble (Fig. 5) to generate another deformation mode—if a truly cylindrical bubble was created, then  $\rho_2$  would be very large, and a plane strain deformation would occur. In Fig. 5, we see that there is some curvature in the  $z$  (axial) direction. However, in this case,  $\rho_2 \sim 230$  mm, whilst  $\rho_1 \sim 20$  mm at the middle section. We then find from Eq. 5.

$$\sigma_1 \sim \frac{\rho_1 \Delta p}{\delta} - 0.09\sigma_2 \quad (7)$$

Because  $\sigma_2$  is about  $0.6\sigma_1$ , at small strains and much less than that at strains of  $O(1)$ , then except at very small strains, the second right-hand side term is less than 5% of

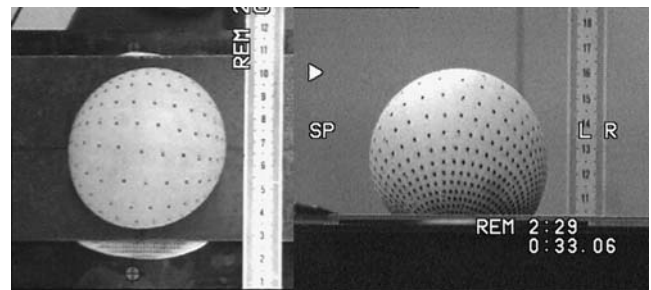
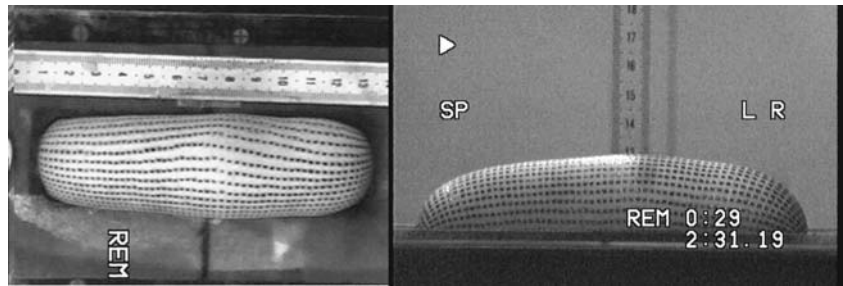


**Fig. 4** Spherical bubble showing the strain pattern. The top profile of the bubble is almost exactly spherical. Stresses are calculated at the pole

**Fig. 5** Rectangular or sausage bubble. The bubble is much less stable than the spherical case, and some axial strain is evident. Stresses are calculated at the mid-section



the first. The sausage bubble experiments are difficult, as the sausage is not always stable, and it is hard to justify any greater accuracy, so the second term on the right-hand side of Eq. 7 is ignored henceforth.

Thus, the experiments can be used to estimate  $\sigma_1$  in both the spherical and sausage bubbles. From the deformation pattern on the surface, the strains at the top of the bubbles can be found. They are plotted in Figs 6 and 7 for the spherical and sausage bubbles, respectively. The strain rate is not constant, but in fact, this is not very important, as stresses vary only as  $\dot{\epsilon}^p$  (Tanner et al. 2008) and  $p \sim 0.22$  for the present case. We assume that the dough is incompressible (Wang et al. 2006), and hence the thickness  $\delta$  at the crown of the bubbles is estimated making this assumption.

To estimate the thickness  $\delta$ , we note that Charalambides et al. (2006) measured  $\delta$  directly using an optical technique. They found that the thickness calculated by Bloksma (1957), which is given by

$$\frac{\delta}{\delta_0} = \left(1 + \frac{h^2}{a^2}\right)^{-2} \quad (8)$$

did not agree well with their measurements. In this equation,  $\delta_0$  is the original sheet thickness before stretching,  $h$  is the bubble height and  $a$  is the original sample radius. In the present case, the thickness at the pole was estimated by

measuring the extension ratios from the dot patterns (see Figs. 4 and 5) and assuming incompressibility (Wang et al. 2006). Hence, if the extension ratios in the  $x$  and  $y$  directions are  $\lambda_x$  and  $\lambda_y$ , respectively, then

$$\frac{\delta}{\delta_0} = \frac{1}{\lambda_x \lambda_y}. \quad (9)$$

It should be mentioned that because the thickness is so critical, it is absolutely necessary to calibrate the optical system to account for the fact that the top of the bubble is closer to the lens than the scales visible in Figs. 4 and 5. For a 60-mm bubble height, there is about a 7% difference in the measurements because of this factor, giving about 14% correction to the thickness. Using Eqs. 8 and 9, the curves shown in Fig. 8 are found; the Bloksma formula is quite close to the inferred measurements from the strains.

In our experiments (Fig. 4), the bubbles are quite spherical; in the Charalambides et al. (2002a) experiments, the bubbles were spheroidal. Because the Bloksma (1957) analysis assumes a spherical bubble, it is perhaps not surprising that Charalambides et al. (2002a) did not find their measured thickness agreeing with Eq. 8.

The radii of curvature at the poles were found from the photographs, the pressure  $\Delta p$  was measured, and the stresses were calculated from Eqs. 6 and 7. Overall, we

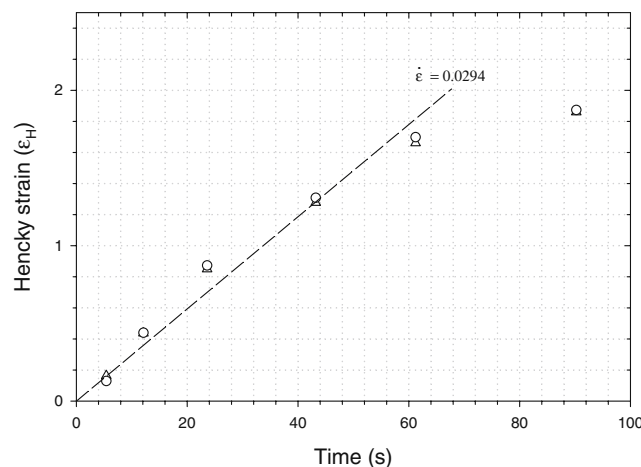


**Fig. 6** Strain as a function of time for the spherical bubble. Note the coincidence of the two strains measured from the  $x$  and  $y$  directions on the grid. The dashed line is an average rate of extension; Eq. 10 is a fitted curve to the data where  $\dot{\epsilon}$  is allowed to vary

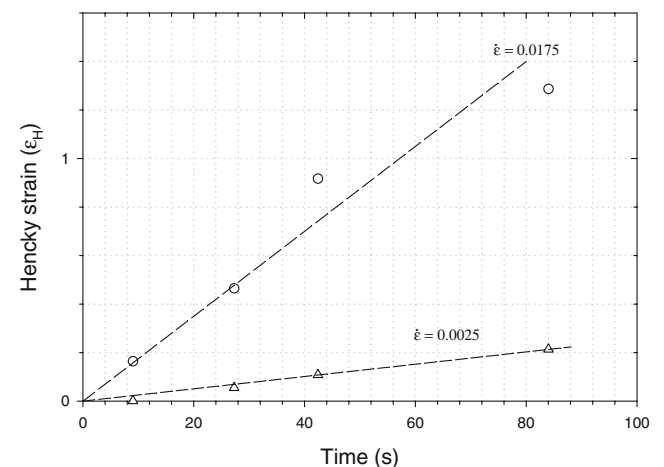


**Fig. 7** Strains at the mid-section of the sausage bubbles. The largest (circumferential) strain rate is about  $0.0175 \text{ s}^{-1}$ , whereas the axial strain is much less ( $\sim 0.0025 \text{ s}^{-1}$ ). In this figure, a constant strain rate in both directions was assumed in computations

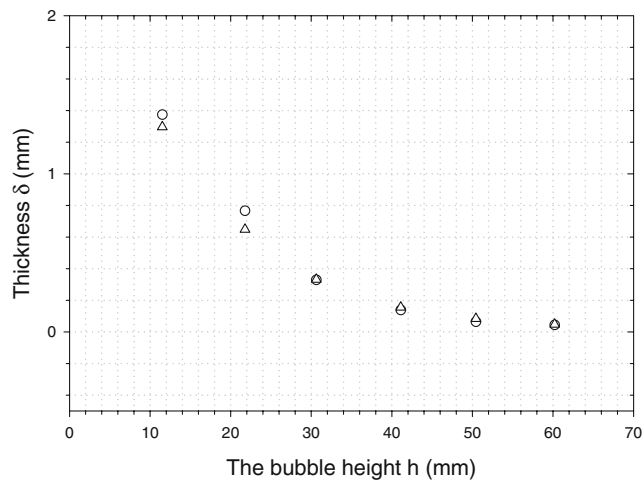


**Fig. 8** Spherical bubble crown thickness as a function of bubble height  $h$ . The *circles* are measurements, and the *triangles* are from the Blokma (1957) theory given in Eq. 8

believe that the accuracy of the stresses was of the order of  $\pm 5\%$ . The final thickness after unloading was also measured, but because recoil occurs, this value considerably exceeds the stretched thickness.

For the analysis, we have assumed  $p=0.22$ ,  $G(1)=14.2$  kPa  $s^p$ , and  $f$  is given by Eq. 4. A 14-mode approximation to the continuous spectrum implied by Eq. 2 was used (Table 2), as in Tanner et al. (2007). The details of the calculation are given in the Appendix. If we pick an average rate of extension for the spherical bubble of  $0.0294$  s<sup>-1</sup>, then the results are as shown in Fig. 9. Using a fit to the elongation rate of

$$\dot{\epsilon} = 0.0432e^{-0.18t}, \tag{10}$$

the results then obtained are also shown in Fig. 9. Because the stresses are not very sensitive to the changes in  $\dot{\epsilon}$ , both the constant and variable  $\dot{\epsilon}$ , as in Eq. 10, give almost identical results (Fig. 9). The divergence between the

**Table 2** Discrete 14-mode spectra for dough  $G(1)=14.2$  kPa  $s^p$ ,  $p=0.22$

Relaxation time $\lambda_i$ (s)	Modulus $g_i$ (Pa)
0.00316	14,017.56
0.01	10,879.37
0.0316	8,446.42
0.1	6,555.47
0.316	5,089.47
1.0	3,950.06
3.16	3,066.71
10.0	2,380.15
31.6	1,847.87
100.0	1,434.18
316.2	1,113.30
1,000.0	864.18
3,162.0	670.83
10,000.0	2,326.84

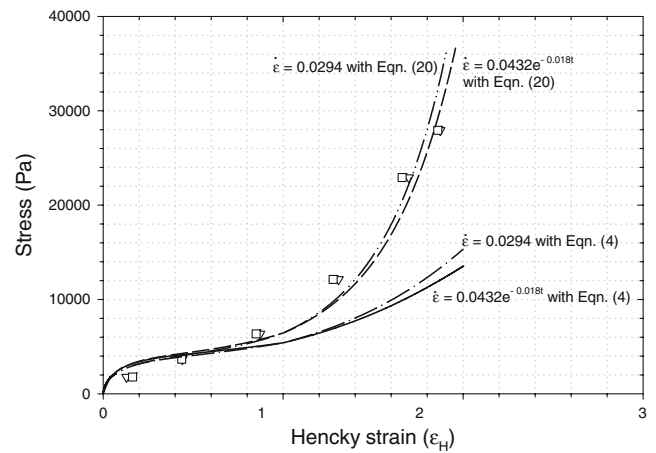


**Fig. 9** Measured and computed stresses for spherical bubbles using a constant mean extension rate ( $0.0294$  s<sup>-1</sup>) and variable rate in Eq. 10. The two *symbols* are from the experimental  $x$  and  $y$  stretches, respectively; they should be equal. Clearly, the use of Eq. 4 for the damage function (*lower curves*) underestimates the stresses by about 100%. The *upper curves* use the modified damage function of Eq. 20

experiments (symbols) and the calculations at large strain using Eq. 4 (lower curves) is to be noted. We shall return to this point latter.

For the sausage bubble  $\dot{\epsilon}_2 \sim 0.143\dot{\epsilon}_1$  (Fig. 7). The agreement of the stresses with the computations in this case is good (Fig. 10), considering the difficulties in experimentation in this case.

### Step strain behaviour

The damage function concept implies that after a strain  $\epsilon_H$ , the material is irretrievably damaged and never recovers. In the case of recoil (Tanner et al. 2007), we found that while this was broadly true, improved recoil predictions were obtained if the contribution of the ‘damaged’ portions

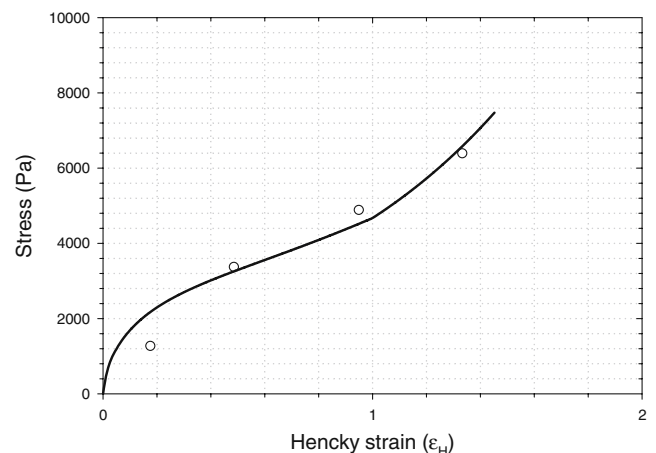


**Fig. 10** Measured and computed circumferential stresses for the sausage bubble using Eq. 4 for the damage function and constant rate of elongation

of the material were considered. Similarly, one might ask if spontaneous ‘healing’ of the network occurs as time progresses (Hibberd and Wallace 1966).

Therefore, in an attempt to probe the damage function concept further, we subjected the dough to a set of step changes in strain. In the first sequence, the 2-mm-thick sample was subjected to an on–off shear strain of 10% on a Paar Physica MCR301 rheometer (Fig. 11). In this instrument, the rise time was about 10–20 ms, so the steps are quite steep. Parallel plates with sandpaper to avoid slip were used, and all stresses and strains refer to the 3/4-Plate radius section (Shaw and Liu 2006). Delay times before reversing were 10, 100 and 1,000 s; Fig. 11 shows the 100-s delay sequence. The stresses measured are shown in Figs. 12, 13 and 14, and the agreement with the computations is adequate; in this case, the  $f$  value is simply that for a Hencky strain of  $\gamma/2$  or  $\epsilon_H \sim 0.05$  after the first step. The failure to capture the extreme experimental stresses directly after the steps is noted; it is believed to be due to the machine dynamics.

For series of increasing step strains with variable delays (Fig. 15), one would expect that the appropriate  $f$  value would change and that the later steps would show a reduction in stress because of a reduction in  $f$ . The results using a variable  $f$  as in Eq. 4 are in Figs. 16 and 17; if  $f$  is held constant in the computations after the first step, then results are as in Figs. 18 and 19.

Clearly, the results of using Eq. 4 (Figs. 16 and 17) are superior to these when  $f$  is equal to the constant (Figs. 18 and 19). Hence, there does not seem to be any significant ‘healing,’ at least on the scale of times of order  $10^3$  s. This will exceed the times relevant to most processing operations, so we shall be content with the use of Eq. 4 in this kind of deformation.

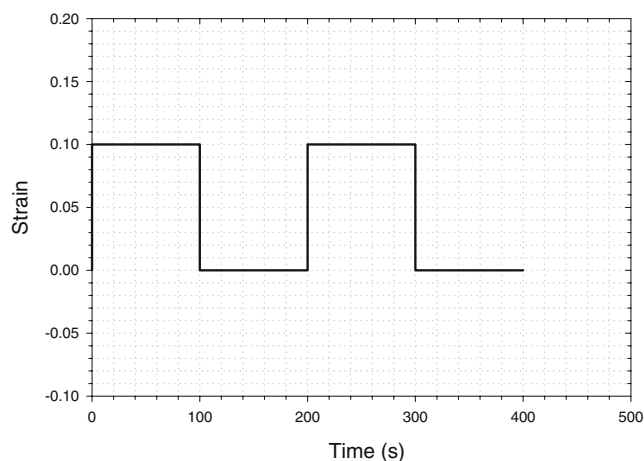


**Fig. 11** Step strain (on–off) pattern. The rise and fall times are about 20 ms, so the steps are steep

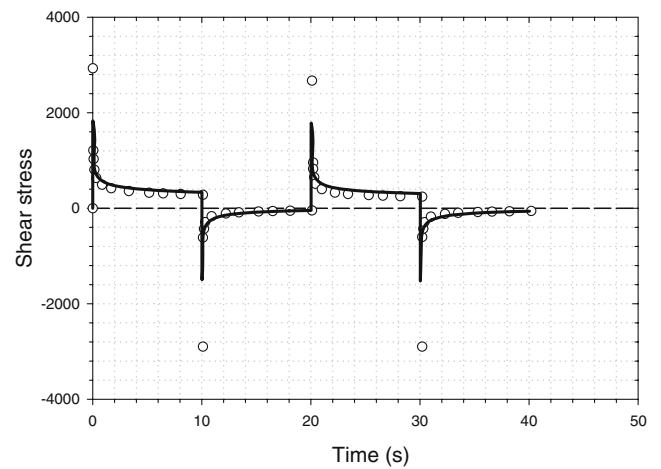


**Fig. 12** Showing agreement between theory and experimental measurements for on–off strain pattern. The calculations use the damage function of Eq. 4 and a 10-s delay time. Symbols are experimental measurements, and the line represents calculated results

### Further consideration of the damage function

From the above and from our previous work, we have shown that the simple  $f(\epsilon_H)$  damage function gives reasonable results in all deformations except the biaxial strain at the pole of spherical bubble, where the actual stresses are around double these predicted from the simple model. We are therefore forced to consider a more complex damage model in this case.

Considering a purely elastic incompressible body, then the stored strain energy  $W$  is given by (Treloar 1958)

$$W = W(I_1, I_2) \tag{11}$$

where  $I_1$  and  $I_2$  are the invariants of the three stretches  $\lambda_x$ ,  $\lambda_y$  and  $\lambda_z$ , given by, in the incompressible case,

$$I_1 = \lambda_x^2 + \lambda_y^2 + \lambda_z^2 \tag{12}$$

$$I_1 = \lambda_x^{-2} + \lambda_y^{-2} + \lambda_z^2 \tag{13}$$

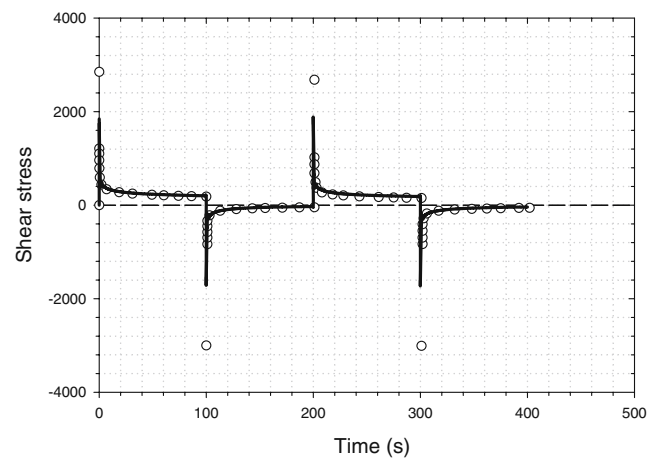


**Fig. 13** As for Fig. 12, with a delay time of 100 s

and

$$\lambda_x \lambda_y \lambda_z = 1 \tag{14}$$

Because dough is very elastic, especially at large strains, we shall suppose that the damage function  $f$  is also a function of  $I_1$  and  $I_2$ . A simple example of Eq. 11 containing  $I_1$  and  $I_2$  is obtained by separating the invariants and assuming a damage function of the form

$$f = f_1(I_1 - 3) + f_2(I_2 - 3). \tag{15}$$

Previously, we have simply used a function of  $\epsilon_H$ ; in these cases, as  $\epsilon_H$  (the Hencky strain) is a function of  $\lambda_{\max}$  ( $\equiv \lambda_x$ , say), then

$$I_1 = \lambda_{\max}^2 + \lambda_y^2 + \frac{1}{\lambda_{\max}^2 \lambda_y^2} \tag{16}$$

and one can consider that using the Hencky strain based on  $\lambda_{\max}$  is nearly equivalent to using  $f$  as a function of  $I_1$  only, as  $\lambda_{\max}^2$  is greater than the other terms in Eq. 16.

Therefore, we will write

$$f = f_1(\epsilon_H) + f_2(I_2 - 3) \tag{17}$$

We can write the invariants  $I_1$  and  $I_2$  for elongation and biaxial extension as follows:

$$\begin{aligned} \text{Elongation} \quad I_1 &= \lambda^2 + \frac{2}{\lambda} \\ I_2 &= \frac{1}{\lambda^2} + 2\lambda \end{aligned} \tag{18}$$

$$\begin{aligned} \text{Biaxial deformation} \quad I_1 &= 2\lambda^2 + \frac{1}{\lambda^4} \\ I_2 &= \frac{2}{\lambda^2} + \lambda^4 \end{aligned} \tag{19}$$

In Eq. 18,  $\lambda$  is the longitudinal extension ratio, and in Eq. 19, it is the in-plane stretch ratio. Note that the biaxial  $I_1$  increases very rapidly compared with all other  $I_1$  and  $I_2$ .

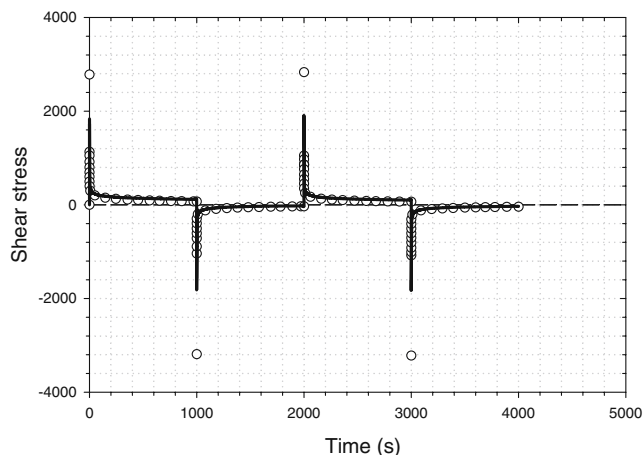


Fig. 14 As for Fig. 12, with a delay time 1000 s

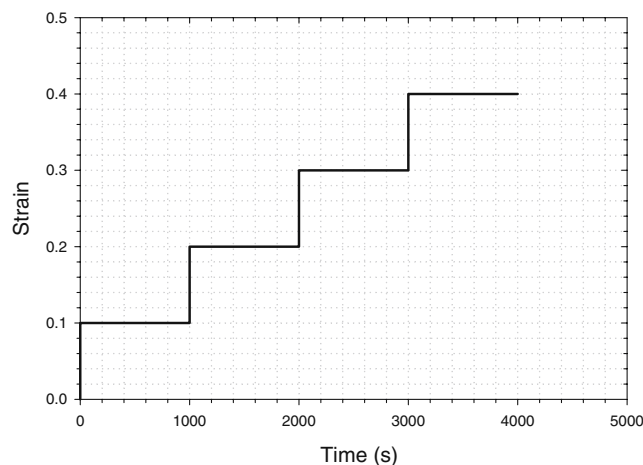


Fig. 15 ‘Stair case’ step strain test; the delay here is 1,000 s

We can fit the biaxial data reasonably well by assuming

$$f = f_R + f_2(I_2 - 3) = f_R + 0.0075(I_2 - 3)^{1/3} \tag{20}$$

In this equation,  $f_R$  is a function of the Hencky strain; it is less than  $f$  (Eq. 4), and  $f_R$  is chosen so that in uniaxial extensions  $f_R + f_2$  is equal to  $f$  in Eq. 4, where no  $f_2$  is assumed.

In the range  $\epsilon_H = 10^{-4} - 1.0$ ,  $f_2$  can be represented by

$$f_R = 0.082 - 0.23 \log \epsilon_H \tag{21}$$

and in the range  $\epsilon_H = 1.0 - 2.2$ , we have

$$f_R = 0.082 - 0.176 \log \epsilon_H. \tag{22}$$

For a large Hencky strain  $\epsilon_H$ ,  $f_R = 0$ . It remains to be seen how this modification affects other deformation patterns. The results are shown in Table 3. Because  $f_R$  plus the uniaxial  $f_2$  for the uniaxial extension is made equal to the  $f$

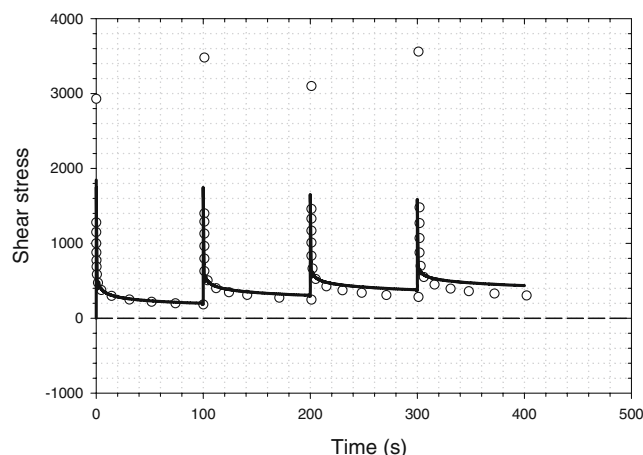
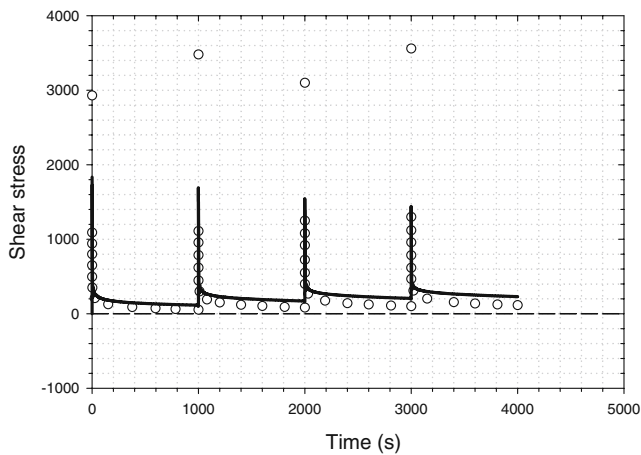


Fig. 16 Response to stair case strain with a 100-s delay. Stresses are computed using the damage function Eqn. 4. Symbols are experimental measurements, and the line represents calculated results





**Fig. 17** As for Fig. 16, but using a 1,000-s delay

( $\epsilon_H$ ) of Eq. 4, the uniaxial results are not changed. The revised  $f$  for the biaxial case and the resulting stresses are also shown; Fig. 9 (upper curves) shows a much better agreement with the resulting stresses.

The biaxial and uniaxial cases represent the extremes of homogeneous deformation (Bird et al. 1987; see their Fig. 8.3—1), but we have also considered the plane strain/shear case, which is an intermediate deformation. In this case,  $\lambda_z=1$ ,  $\lambda_x=\lambda$ ,  $\lambda_y=1/\lambda$ , and

$$I_1 = I_2 = 1 + \lambda^2 + \frac{1}{\lambda^2} \tag{23}$$

The calculation of  $f_2$  using Eqs. 20 to 22 shows that this case is close to the uniaxial case—for example,  $f_2=0.018$  at  $\epsilon_H=2$  for uniaxial elongation and 0.028 for the plane strain case. There is no dramatic upturn as in the biaxial case. This confirms that the simple  $\epsilon_H$  from Eq. 4 is useful for

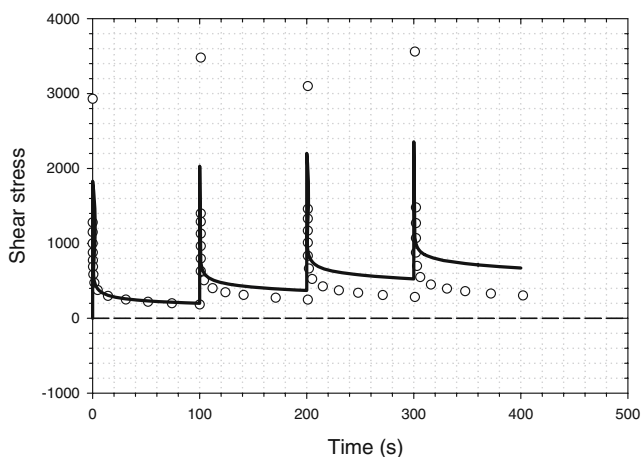


**Fig. 18** As for Fig. 16, but here the damage function  $f$  is maintained at the same value ( $\sim 0.39$ ) that it acquires after the first step. The agreement with experiment is worse than in Fig. 16

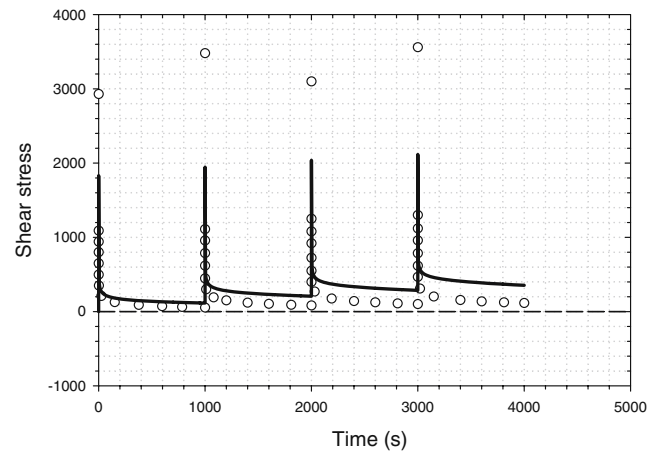


**Fig. 19** As for Fig. 18, with a 1,000-s delay

shear, plane strain and the sausage bubble case but not for the biaxial deformation, where Eqs. 20 to 22 are preferred.

### Conclusions

The present paper continues the exploration of the simple Lodge model plus damage function concept begun in previous papers. Applied to a typical Australian bread dough, we have shown in previous papers that the model can describe

1. Small strain behaviour
2. Steady shear behaviour beginning from rest
3. Steady elongational behaviour
4. Stress relaxation in shear
5. Recoil, with application to sheeting
6. Reasonable predictions of moderate sinusoidal inputs (up to 30% strain) at various frequencies

In the present paper, we have considered step strain histories ( $\sim 10\%$  strain levels), and these show that the damage concept remains relevant. However, predictions of stresses in biaxial stretching were far too low. By reconsidering the damage function as a function of the two invariants of strain, instead of the theory strain based on the largest stretch only, we are able to fit the biaxial data as well as all the other cases mentioned above.

The approach of modifying the damage function is not the only possible one. One obvious idea is to replace the  $C^{-1}$  tensor in Eq. 1 by a combination of  $C^{-1}$  and  $C$ , thus giving a Mooney-type material response and a second normal stress difference (Tanner 2000). However, we presently have no measurements of the second normal stress difference for dough, so we have not pursued this idea. We would prefer to have a soundly based ‘molecular’ theory to clarify the concepts, but none is presently available. We hope that further work on the concept will

**Table 3** Modified damage function

$\varepsilon_H$	$\lambda$	$f(\varepsilon_H)$ (Eq. 4)	$I_2-3$ (uniaxial)	$I_2-3$ (biaxial)	$f_R$	$f_2$ (Eq. 20, biaxial)	Revised $f$ , $f=f_R+f_2$ (biaxial)	$\sigma$ , kPa (biaxial, $\dot{\varepsilon} = 0.0294$ )
0	1.0	1.0	0	0	1.0	0	1.0	0
0.5	1.649	0.16	0.67	5.13	0.153	0.013	0.166	4.2
1.0	2.718	0.092	2.57	51.8	0.082	0.028	0.11	6.4
1.5	4.48	0.065	6.01	400	0.051	0.055	0.106	14.6
2.0	7.39	0.046	11.8	2980	0.029	0.108	0.137	45.8
2.5	12.18	0.031	21.4	22005	0.01	0.21	0.22	186

be forthcoming—there appears to be considerable scope for introducing the damage concept into soft solid rheology.

**Acknowledgements** We thank the Australian Research Council for funding the research and Drs. F. Békés and M.P. Newberry of CSIRO for their advice, assistance and criticism.

## Appendix

### Calculations of the stress response

In the present work, the stresses have been calculated for uniaxial extension, biaxial extension (bubble tests) and sets of step changes in shear strain (step shear—on—off and a staircase of increasing step strains, with variable delays) by using the model described above. In the calculations, the 14-mode spectra  $\lambda_i$  and  $g_i$  have been used (note: in this Appendix, the symbol  $\lambda$  denotes a relaxation time). The relaxation times are evenly spaced (here, 0.5 decade is adopted) and the modulus  $g_i$  is then given by Tanner et al. (2007, 2008; Qi et al. 2008) for the power-law spectrum corresponding to the memory function of Eq. 2

$$g_i = H(\lambda_i) \frac{r^{p/2} - r^{-p/2}}{p} \quad (24)$$

where  $\lambda_i$  is the corresponding relaxation time and the longest one is 10,000 s,  $r = \lambda_{i+1}/\lambda_i$  (here,  $r=3.162$ ),  $p$  is a power-law exponent depending on the dough (defined in Eq. 2),  $H(\lambda_i)$  is the relaxation spectrum corresponding to Eq. 2 and it is of the form (Pipkin 1986)

$$H(\lambda_i) = \frac{G(1)\lambda_i^{-p}}{(p-1)!} \quad (25)$$

in which  $G(1)$  is a constant that can be numerically evaluated by the relaxation function at  $t=1$  s, but it has a different dimension from modulus  $G$  (Tanner et al. 2007, 2008; Qi et al. 2008). We prefer, as do the Jeffreys and Jeffreys (1956), and Pipkin (1986), the factorial function (!) notation to that of the closely related gamma function  $x! = \Gamma(x+1)$ , if only because it is neater. Tables of the factorial and gamma functions for non-integer values (positive and

negative) are given by Abramowitz and Stegun (1965). The values of  $\lambda_i$  and  $g_i$  are shown in Table 2.

In the computations, the differential equation of the UCM model has been adopted as the constitutive equation, which is exactly equivalent to the integral form of Lodge's model (Tanner 2000). The equation of the UCM model is given by

$$\lambda \frac{\Delta \boldsymbol{\tau}}{\Delta t} + \boldsymbol{\tau} = 2\eta \mathbf{d}. \quad (26)$$

in which, for each of the 14 modes,  $\Delta/\Delta t$  is the usual upper convected time derivative (Tanner 2000),  $\boldsymbol{\tau}$  is the stress tensor,  $\lambda$  is the relaxation time,  $\eta$  is the viscosity and  $\mathbf{d}$  is the rate of deformation tensor which equals  $(\mathbf{L} + \mathbf{L}^T)/2$ . The velocity gradient tensor  $\mathbf{L}$  is defined as  $\mathbf{L} = (\nabla \mathbf{v})^T$  or  $L_{ij} = \partial v_i / \partial x_j$ , where  $\mathbf{v}(x, t)$  is the velocity field at place  $\mathbf{x}$  at time  $t$ . The upper convected derivative  $\Delta/\Delta t$  is defined as

$$\frac{\Delta \boldsymbol{\tau}}{\Delta t} \equiv \frac{\partial \boldsymbol{\tau}}{\partial t} + (\mathbf{v} \nabla) \boldsymbol{\tau} - \boldsymbol{\tau} \mathbf{L}^T - \mathbf{L} \boldsymbol{\tau}. \quad (27)$$

### Step shear flow

According to the experimental setting, the shear rate used in applying the steps  $\dot{\gamma} = 10 \text{ s}^{-1}$ . For every single mode  $\lambda_i$  and  $g_i$ , the corresponding shear stress  $\tau_i$  can be obtained by numerically solving Eq. 26 by using a Runge–Kutta numerical analysis method/or directly from the solution of Eq. 26. Then, the total shear stress is the sum of the partial stresses

$$\tau_{\text{UCM}} = \sum_{i=1}^{14} \tau_i. \quad (28)$$

The shear stress is therefore determined by multiplying Eq. 28 by  $f$ :

$$\boldsymbol{\tau} = f \tau_{\text{UCM}} \quad (29)$$

where  $f$  is the damage function defined in Eq. 4, as a function of the Hencky strain  $\varepsilon_H$ . The Hencky

strain  $\varepsilon_H$  is related to the shear strain  $\gamma$  by (Kitoko et al. 2003)

$$\varepsilon_H = \frac{1}{2} \ln \left[ 1 + \frac{\gamma^2}{2} + \gamma \sqrt{1 + \frac{\gamma^2}{4}} \right]. \quad (30)$$

In the calculations of the shear stress for step shear–relaxation-step shear (reversing) flow, the damage function  $f$  is set to be a constant after the first step shear, which is set to be the value of the  $f$  function at the final state of the first step shear because the next step shear is in the reverse direction. We used both  $f$  as a constant after the first step of shear and as a continuous function of the strain in the calculations for the staircase with increasing step strains, for comparison.

### Uniaxial elongation and biaxial extension

For the extensional flows, the rate of the deformation tensor in Eq. 26 is defined as

$$\mathbf{d} = \dot{\varepsilon} \begin{bmatrix} 1 & 0 & 0 \\ 0 & q & 0 \\ 0 & 0 & -(1+q) \end{bmatrix}. \quad (31)$$

where  $q$  is a constant, and it depends on the deformation tensor. For the elongational flow  $q=-0.5$ , biaxial (on the top of the spherical bubble)  $q=1$ , and according to the experimental measurements, we found that  $q=0.143$  for the case of the sausage bubble (Fig. 7). The partial stresses  $\sigma_1^i$  and  $\sigma_3^i$  of the  $i$ th mode can be therefore calculated by solving the Eq. 26. Then, the response stress is given by

$$\sigma = f \sum_{i=1}^{14} (\sigma_1^i - \sigma_3^i). \quad (32)$$

### References

- Abramowitz M, Stegun IA (1965) Handbook of mathematical functions. Dover, New York
- Bird RB, Armstrong RC, Hassager O (1987) Dynamics of polymeric liquids: fluid mechanics, vol. 1. 2nd edn. Wiley, New York
- Bloksma AH (1957) A calculation of the shape of the alveograms of some rheological model substances. *Cereal Chem* 34:126–136
- Bloksma AH (1990) Dough structure, dough rheology, and baking quality. *Cereal Foods World* 35:237–244
- Charalambides MN, Wanigasooriya L, Williams JG, Chakrabarti S (2002a) Biaxial deformation of dough using the bubble inflation technique, I. *Experimental Rheol Acta* 41:532–540
- Charalambides MN, Wanigasooriya L, Williams JG (2002b) Biaxial deformation of dough using the bubble inflation technique, II. Numerical modelling. *Rheol Acta* 41:541–545
- Charalambides MN, Wanigasooriya L, Williams JG, Goh SM, Chakrabarti S (2006) Large deformation extensional rheology of bread dough. *Rheol Acta* 46:239–248
- Dobraszczyk B, Morgenstern MP (2003) Rheology and the breadmaking process. *J Cereal Sci* 38:229–245
- Hibberd GE, Wallace WJ (1966) Dynamic viscoelastic behaviour of wheat flour doughs. *Rheologica Acta* 5:193–198
- Jeffreys H, Jeffreys BS (1956) Methods of mathematical physics, 3rd edn. Cambridge University Press, Cambridge (see Chapter 15)
- Kitoko V, Keentok M, Tanner RI (2003) Study of shear and elongational flow of solidifying polypropylene melt for low deformation rates. *Korea–Australia Rheol J* 15:63–73
- Lodge AS (1964) Elastic liquids. Academic, London
- Ng TSK, McKinley GH, Padmanabhan M (2006) Linear to non-linear rheology of wheat flour dough. *Appl Rheol* 16:265–274
- Pipkin AC (1986) Lectures on viscoelasticity theory, 2nd edn. Springer, New York
- Qi F, Dai SC, Newbery MP, Love RJ, Tanner RI (2008) A simple approach to predicting dough sheeting thickness. *J Cereal Sci* (in press)
- Shaw MT, Liu ZZ (2006) Single-point deformation of nonlinear rheological data from parallel-plate torsional flow. *Appl Rheol* 16:70–79
- Tanner RI (2000) Engineering rheology, 2nd edn. Oxford University Press, Oxford, UK
- Tanner RI, Dai SC, Qi F (2007) Bread dough rheology and recoil 2. Recoil and relaxation. *J Non-Newton Fluid Mech* 143:107–119
- Tanner RI, Qi F, Dai SC (2008) Bread dough rheology and recoil 1. Rheology. *J Non-Newton Fluid Mech* 148:33–40
- Treloar LRG (1958) The physics of rubber elasticity, 2nd edn. Oxford University Press, Oxford
- Wang C, Dai SC, Tanner RI (2006) On the compressibility of bread dough. *Korea–Australia Rheol J* 18:127–131